Atmospheric Research 265 (2022) 105886

Contents lists available at ScienceDirect

Atmospheric Research

journal homepage: www.elsevier.com/locate/atmosres

Characterization of dust activation and their prevailing transport over East Asia based on multi-satellite observations

Minghui Tao [a,*], Liangfu Chen [b], Jun Wang [c], Lili Wang [d], Wencai Wang [e], Changqing Lin [f], Lu Gui [a], Lunche Wang [a], Chao Yu [b], Yi Wang [a]

[a] *Key Laboratory of Regional Ecology and Environmental Change, School of Geography and Information Engineering, China University of Geosciences, Wuhan 430074, China*
[b] *State Key Laboratory of Remote Sensing Science, Aerospace Information Research Institute, Chinese Academy of Sciences, Beijing 100101, China*
[c] *Center for Global and Regional Environmental Research, The University of Iowa, Iowa City, IA 52242, USA*
[d] *State Key Laboratory of Atmospheric Boundary Layer Physics and Atmospheric Chemistry, Institute of Atmospheric Physics, Chinese Academy of Sciences, Beijing 100029, China*
[e] *Key Laboratory of Physical Oceanography, College of Oceanic and Atmospheric Sciences, Ocean University of China, Qingdao 266100, China*
[f] *Division of Environment and Sustainability, The Hong Kong University of Science and Technology, Hong Kong 999077, China*

ARTICLE INFO

Keywords:
Dust transport
Satellite
Dust-pollution mixing
East Asia

ABSTRACT

Mineral dust from the deserts and arid areas in East Asia plays a critical role in regional climate and air quality. Based on integrated satellite observations and MERRA-2 reanalysis, we provide an observational insight into dust activities governing spatial patterns of dust aerosols over East Asia. With Moderate resolution Imaging Spectroradiometer Aerosol Optical Depth (AOD) and Ozone Monitoring Ultraviolet Aerosol Index (UVAI), fixed dust-active areas with distinct spatial-temporal differences are revealed. Besides the few dust storms mostly in spring, unnoticeable but frequent dust plumes are found to be the predominant sources of prevailing dust particles over East Asia. Compared with the active dust sources in Taklimakan Desert throughout the year, dust activities in Gobi deserts are at a much lower frequency. The elevated dust plumes are concentrated within 2–6 km over the deserts with large seasonal variations, and can be transported downstream to eastern China and Sichuan Basin within 3–5 days. Moreover, owing to the lack of enough strong winds, these dust plumes tend to be concentrated above the haze layers near surface in eastern China. The intense temperature inversion during winter and early spring can delay the mixing of dust-pollution. Despite a generally reasonable performance in dust AOD, MERRA-2 reanalysis exhibits some uncertainties in reproducing spatial locations of dust hotspots, dust concentration, and transport process. Our results emphasize significant role of the inapparent but prevalent dust plumes in air quality and in climate effects of East Asia.

1. Introduction

Mineral dust, one of the major components of aerosols in the atmosphere, transports and transforms materials and energy of the Earth system in several different ways. Strong winds usually lift massive dust particles into atmosphere from deserts and arid areas of the world and carry them regionally or even globally in atmospheric circulation (Kim et al., 2019; Wang et al., 2021; Wu et al., 2020; Yu et al., 2012). These elevated dust aerosols can alter solar radiation balance (Wang et al., 2020b) and modify cloud properties (Huang et al., 2006), exerting significant influences on regional climate (Huang et al., 2014). Moreover, long-range transport of desert dust aggravates air quality in downstream urban/industrial areas, as well as provides a reactive surface in troposphere photochemistry (Dentener et al., 1996). Additionally, mineral dust deposited over the ocean is an important nutrient in biogeochemistry and carbon cycles (Jickells et al., 2005).

Dust events over East Asia have been a focus of numerous studies regarding climate and air quality due to their widely influences (Guo et al., 2017; Jin et al., 2021a; Kim et al., 2019; Ma et al., 2019; Tao et al., 2021; Wang et al., 2020a). The northwestern part of East Asia is dominated by vast arid/semi-arid areas and deserts (Fig. 1), which contribute about half of the desert dust emissions of the world (Wang et al., 2012; Zhang et al., 1997). Every year, large amounts of dust particles transport downstream to the densely populated regions in eastern China, Korea,

* Corresponding author at: NO. 388, Lumo Road, Hongshan District, Wuhan 430074, China.
E-mail address: taomh@cug.edu.cn (M. Tao).

https://doi.org/10.1016/j.atmosres.2021.105886
Received 12 July 2021; Received in revised form 9 October 2021; Accepted 12 October 2021
Available online 15 October 2021

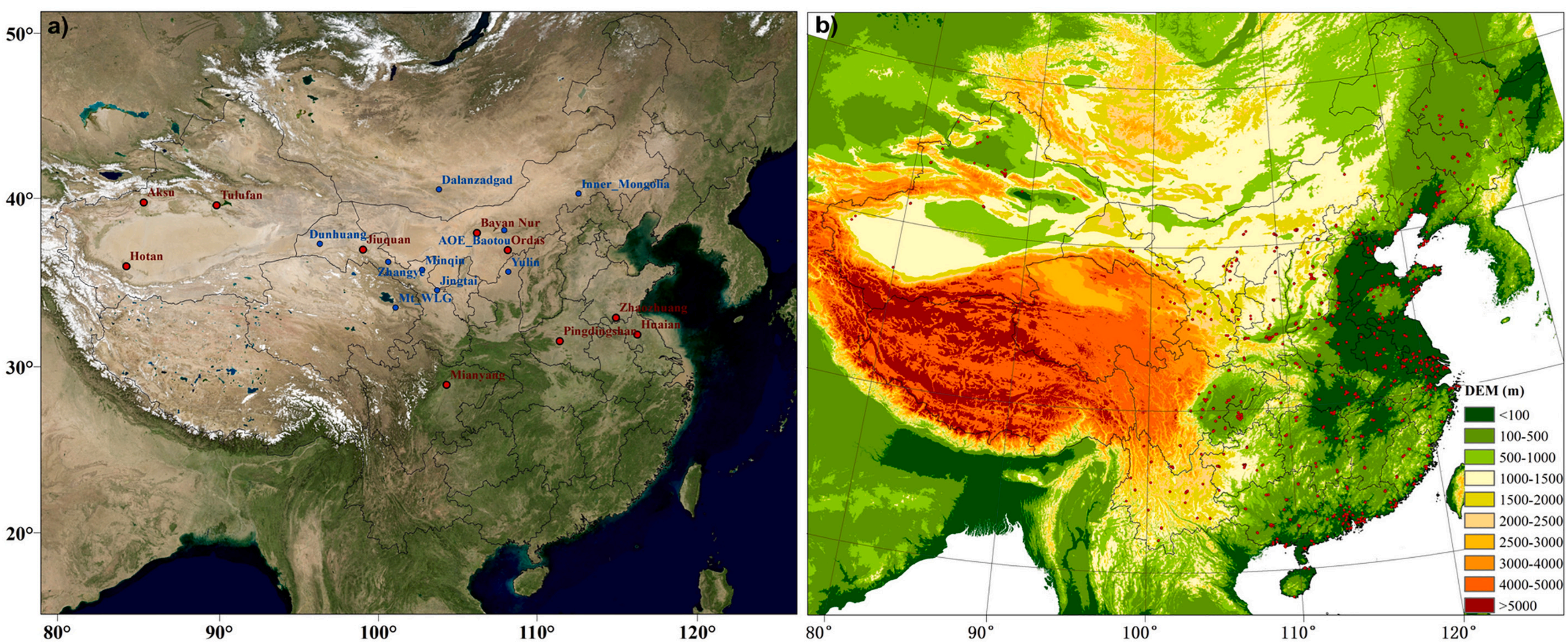

Fig. 1. a) Geographic location of selected AERONET sites (blue) and air quality sites (red) in MODIS true color image, b) Digital Elevation Model (DEM). (For interpretation of the references to color in this figure legend, the reader is referred to the web version of this article.)

and Japan, along with intense dust-pollution interactions (Huang et al., 2010). The prevalent dust particles provide a predominant source of cloud condensation nuclei in spring by pollution-enhanced activation (Ma et al., 2010), and can modify cloud properties (Wang et al., 2010). Moreover, atmospheric heating by Asian dust can be substantially enhanced due to mixing with soot parties during downstream transport (Itahashi et al., 2010; Kim et al., 2005). To quantify the role of dust aerosols in air quality and climate change over East Asia, it is essential to understand how these dust particles change over space and time.

The advent of dedicated satellite instruments for aerosol retrieval over land since late 1990s has greatly renewed the knowledge regarding global distribution of dust hotspots (Ginoux et al., 2012; Omar et al., 2009; Torres et al., 2007). Although the widely used satellite aerosol products such as from Moderate Resolution Imaging Spectroradiometer (MODIS) and Cloud-Aerosol Lidar and Infrared Pathfinder Satellite Observation (CALIPSO) can reveal general spatial patterns of aerosols and their vertical variation, considerable bias of MODIS retrievals in the desert region of East Asia and low frequency of CALIPSO observation hinder further characterization of dust activities (Tao et al., 2019). In particular, the existing observational studies are usually confined to the few large-scale dust storm events, which only account for a very small fraction of the frequent dust activities (Yu et al., 2019; Wu et al., 2020). Tao et al. (2012, 2014) emphasized that dust activities with much smaller scales than dust storms but much higher frequency have a crucial driving effect in formation of abrupt haze pollution in eastern China. So far, several key characteristics of the dust activities over East Asia, including spatial and temporal variability of their scales and intensity, transport potential of different dust sources, and dust events at which scales have dominant contribution to the prevailing dust aerosols, are still unclear.

In this study, we present a large-scale observational insight into dust activities and their downstream transport over East Asia based on multiple satellite observations and MERRA-2 (second Modern-Era Retrospective analysis for Research and Applications) reanalysis. Section 2 introduces the satellite aerosol products, ground measurements, and MERRA-2 reanalysis used. Satellite observation of the frequency of dust activities and their seasonal patterns are shown in section 3.1. Section 3.2 investigates the dust transport with CALIPSO vertical detection. Transport process of a typical dust event as well as performance of MERRA-2 dust reanalysis are analyzed at the daily scales with ground measurements in section 3.3. Also, we discuss the difference of our results with previous studies in section 3.4. Section 4 summarizes our findings and primary conclusions. The main purpose of our work is to provide a general view of the predominant dust activities driving variations of mineral dust over East Asia.

2. Data and methods

2.1. Satellite aerosol data sets

The aerosol products from multi-spectral instrument such as MODIS aboard Terra and Aqua satellite since 2000 and 2002 have been widely used due to their near daily global coverage and high spatial resolution (1–10 km). The recent Collection (C) 6 MODIS Multi-angle Implement of Atmospheric Correction (MAIAC) algorithm can provide reliable AOD retrieval at 1 km over bright surface such as deserts by utilizing minimum reflectance method (Lyapustin et al., 2018; Tao et al., 2019). Besides, Multi-angle Imaging SpectroRadiometer (MISR) measurements onboard Terra since 2000 with additional angular information are sensitive to particle size and shape (Kahn and Gaitley, 2015). Despite an overestimation in high-AOD conditions, the current Version (V) 23 MISR AOD at 4.4 km has a robust performance over the deserts of East Asia for low-moderate values ($<$0.4) (Tao et al., 2020). Since anthropogenic emissions are concentrated in urban/industrial areas, satellite AOD can well indicate dust loading in the desert and arid regions of East Asia with a sparse population. Despite a low temporal resolution, long-term mean of daily V23 MISR AOD during 2008–2018 is utilized to characterize dust loading over the deserts. To examine variations of dust activities, frequency of daily C6 MODIS MAIAC AOD $>$0.1 is used.

The Ozone Monitoring Instrument (OMI) aboard Aura satellite measures Earth-atmosphere's reflectance in ultraviolet (UV) and visible spectra (270–500 nm) with nadir pixel size at 13 $\times$ 24 km and a wide swath width ($\sim$2600 km) (Torres et al., 2007). UV Aerosol Index (UVAI) is an effective indicator of UV-absorbing aerosols by contrast between aerosol absorption and Rayleigh scattering. Despite a qualitative parameter, UVAI is very sensitive to the existence of elevated absorbing aerosols such as airborne dust and biomass burning smoke regardless of surface types, and even aerosols mixed in or above clouds (Herman et al., 1997). As a successor of OMI, Ozone Mapping and Profiler Suite (OMPS) onboard NPP satellite since 2011 has a spectrum range in 300–380 nm at a resolution of 1 nm and a nadir pixel size of 50 $\times$ 50 km. We employ OMI Level (L) 2 gridded UVAI at 0.25° only during 2005–2008 due to OMI row anomalies, and select OMPS products instead after 2011.

Cloud-Aerosol Lidar with Orthogonal Polarization (CALIOP) on CALIPSO satellite since 2006 provides vertical profiles of elastic backscatter of aerosols at 532 and 1064 nm, and separate dust from other aerosol types with high depolarization ratio of nonspherical particles at 532 nm (Omar et al., 2009). The CALIPSO Lidar L3 Tropospheric Aerosol Profile data reports globally gridded, quality-screened, monthly aerosol extinction profiles and layer classification products at 5° $\times$ 2° (Tackett et al., 2018). We select recent V4.20 CALIPSO L3 data in 2007–2018 to characterize vertical variations of dust aerosols. Although CALIPSO has a very close crossing time with MODIS and OMI, CALIPSO nighttime products with less noise are utilized rather than daytime ones. In addition, true color image from NPP VIIRS (Visible infrared Imaging Radiometer) is used for a visible view of general atmospheric conditions in case analysis.

2.2. MERRA-2 aerosol reanalysis

MERRA-2 is a long-term atmospheric reanalysis since 1980 produced by NASA's Goddard Earth Observing System Model, Version 5 (GEOS-5). Also, MERRA-2 is the first satellite-era global reanalysis to assimilate satellite observation of aerosols and Aerosol Robotic Network (AERONET) AODs (Gelaro et al., 2017). Being radiatively coupled to the aerosol module of Goddard Chemistry Aerosol Radiation and Transport model (GOCART), the GEOS-5 model can simulate five types of aerosols including dust, sea salt, sulfate, and black and organic carbon (BC and OC). Besides optical properties including AOD and absorption of these aerosol components, the current V5.12.4 MERRA-2 provides their columnar and surface mass concentrations with hourly temporal resolution at uniform grid of 0.625° $\times$ 0.5°.

Although only AOD is constrained by observations, comparison of MERRA-2 aerosol reanalysis with MODIS AOD, OMI UVAI, and CALIPSO profiles shows reliable performance in a global scale (Buchard et al., 2017). Moreover, hourly MERRA-2 can generally reproduce temporal variations of AODs in AERONET. In the other hand, some limitations such as no treatment of nitrate particles and too-low OC generated in GOCART have led to systematic underestimation of total AOD and mass concentration of particulate matter (PM) in MERRA-2. Since we focus on dust aerosols here, V5.12.4 MERRA-2 dust AOD and mass concentration near the satellite passing time are selected.

2.3. Geography background and ground measurements

As shown in Fig. 1, the landscape in northwestern part of East Asia is characterized by deserts and bare lands. The largest Taklimakan Desert is in a basin surrounding by high mountains ($>$3 km). Thus, a large fraction of the dust emissions just falls back to local source areas due to insufficient uplift height or deposition of coarse particles without continuing strong winds (Chen et al., 2017; Ginoux et al., 2012). By contrast, Gobi deserts are distributed in a relatively flat plateau with an elevation >1 km. Since 2013, the Environment Protection Agency of China establishes national air quality monitoring network (Fig. 1), which releases hourly mass concentration of six atmospheric pollutants including PM with diameters that are generally 10 μm or smaller (PM_{10}), $PM_{2.5}$, sulfur dioxide, nitrogen dioxide, ozone, and carbon monoxide. Though there are no specific sites in dust source areas, we select hourly PM_{10} data in air quality sites around deserts and their downstream regions to examine the influence of dust transports. Similar as validation of satellite AOD (Jin et al., 2021b), hourly PM_{10} and $PM_{2.5}$ measurements from ground sites in the 0.625° × 0.5° MERRA-2 grid are selected to evaluate reanalysis of dust concentration.

2.4. Description of dust activity with satellite observations

The definition and classification of sand and dust weather are usually realized by utilizing meteorological parameters such as visibility and surface wind speed. For instance, the China Meteorological Administration divides sand and dust weather into dust storm, blowing dust, and floating dust, with a visibility <1 km, ranging in 1–10 km, and < 10 km (with also low surface wind speed ≦3 m/s), respectively (http://www.cma.gov.cn/2011xzt/kpbd/Sand/). However, meteorological observation in ground sites can be limited in characterizing elevated dust and their regional transport. On the other hand, satellite observations provide a large-scale view of both dust activities over deserts and their downstream transport, and can identify and quantify spatial scales and intensity of dust events in the deserts and arid areas by AOD and UVAI. To describe long-term dust activities regulating spatial patterns of dust aerosols, “dust plume” defined as a region of optically distinct dust extending from an identified source to a downwind region is used here (Yu et al., 2019). Additionally, we tend to utilize dust storm to denote very thick dust plumes (e.g., AOD >1.0) of heavy dust events in this study.

3. Results and discussion

3.1. Multi-satellite observation of dust activity over East Asia

Although only several dust storm events or less occur in eastern China every year, prevailing dust particles have been observed by both satellite and ground observations (Tao et al., 2014). Fig. 2 shows typical regional haze pollution covered by dust plumes in eastern China on Jan. 19, 2018. High values of OMPS UVAI (>2.0) demonstrate the existence of prevalent UV-absorbing aerosols. Since there are few agriculture burning fires in eastern China during this non-harvest season, these UV-absorbing aerosols can be airborne dust rather than fire smoke. CALIPSO observation passing over the central part of eastern China displays several aerosol layers from near surface to ~8 km. There is a strong extinction layer within 500 m near surface, which can be caused by accumulation of anthropogenic emissions. Besides, two thick dust layers are found above the pollution. The first dust layer is distributed between 0.5 and 2.5 km, and mixes with the atmospheric pollutants when dust particles are transported deep into to polluted areas in eastern China (Fig. 2d). By contrast, the topmost dust layer is concentrated between

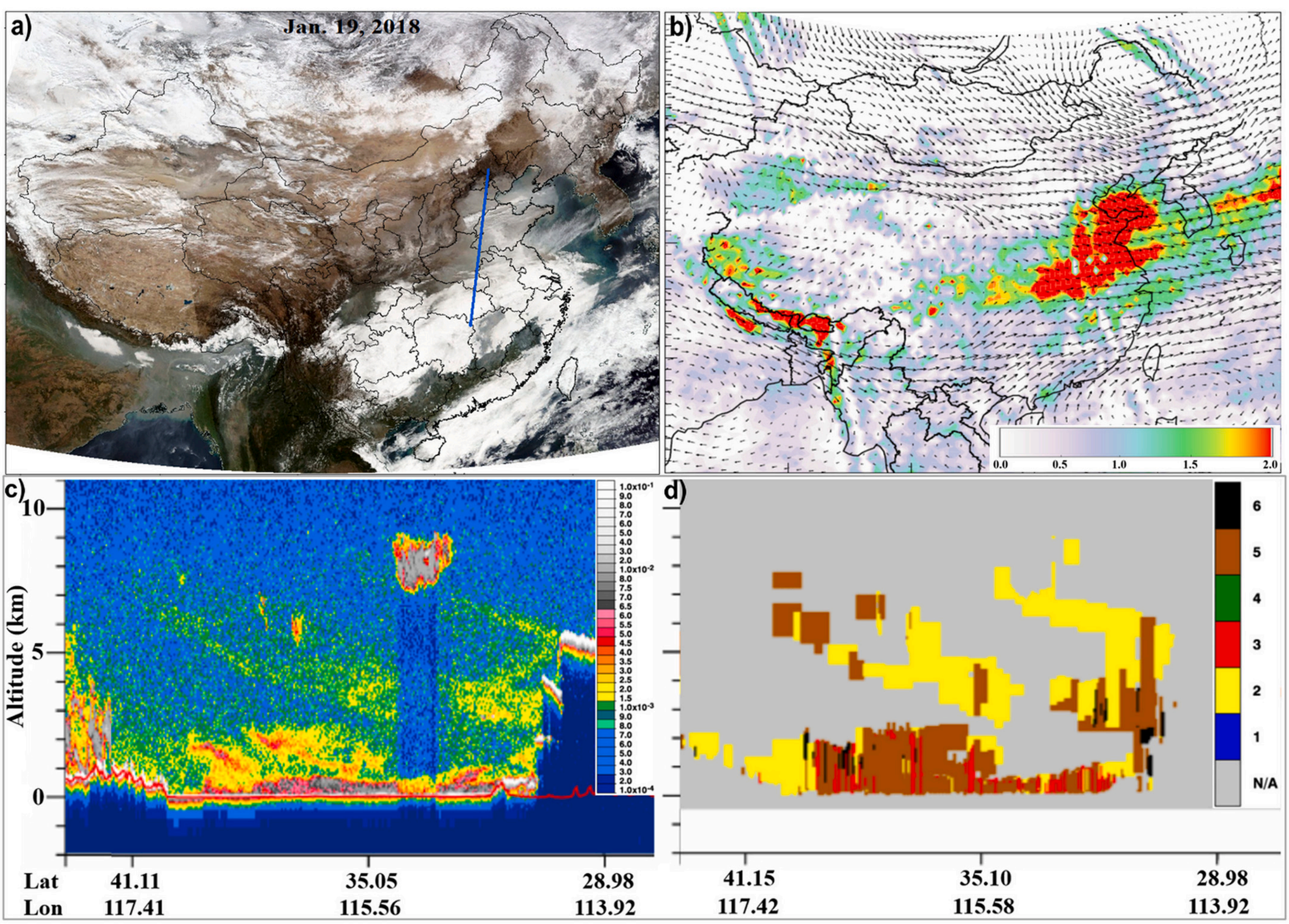

Fig. 2. a) NPP VIIRS true color image, b) OMPS UVAI with winds at 700 hPa, c) CALIPSO backscatter, d) sub aerosol type over eastern China on Jan. 19, 2018.

2.5 and 4.5 km, and its much higher height of ~6–8 km indicates marked potential of long-range transport. These elevated dust plumes tend to usually exist above the haze layers in the eastern part of East Asia during winter (Fig. 1S), which can originate from deserts under the predominant northwestern winds at 700 hPa.

Compared with the large-scale dust storms that are striking in both satellite true color image and ground visual observation, the dust plumes at smaller scales in Fig. 2 are unnoticeable over the bright surface in deserts and haze layers downstream. However, these dust plumes can exert deeper influence on regional atmospheric environment due to a much higher frequency. To inspect spatial patterns of dust loading over deserts and arid areas of East Asia, mean value of MISR AOD during 2005–2018 is analyzed (Fig. 3a). High values of MISR AOD (>0.5) are concentrated at the edge of Taklimakan Desert, and are much higher than in Gobi deserts. There is a clear transport path between northwestern and eastern China with AOD >0.2. To examine dust activation of these deserts, annual frequency of MODIS AOD >0.1 is counted. Dust-active areas are clearly shown with large spatial variations (Fig. 3b). The dust-active areas of Gobi deserts are very scattered with notable difference in frequency and scales. It should be noted that the high frequency of AOD >0.1 along the path of Bayan Nur and Baotou can be attributed to pollution hotspots from cities. In addition, the low values of annual MISR AOD (<0.2) in the Gobi deserts can be partly caused by the relatively low frequency of AOD >0.1.

Despite a qualitative parameter, the sensitivity of OMI UVAI to elevated dust even above cloud/snow makes it an effective indicator of active dust sources. Seasonal frequency of OMI UVAI >1.0 during 2005–2008 displays temporal variations of the dust activities (Fig. 4). Compared with satellite AOD that also reflects urban/industrial pollution hotspots, seasonal UVAI reveals very concentrated dust-active areas in deserts and arid areas of East Asia. Also, there is a high frequency of UVAI >1.0 in downstream northern China during winter (>30 days) and spring (>20 days). Since agriculture fires in eastern China mainly occur in the harvest periods of summer and fall, the frequent UV-absorbing aerosols can be dominated by airborne dust. Meanwhile, UVAI over the Sichuan Basin (SC) exceeds 1.0 for more than 10 days in both winter and spring. It's worth noting that fixed and isolated areas with UVAI >1.0 exist in the west and south of the Tibetan Plateau (TP). Although elevated dust from Taklimakan Desert and South Asia can be transported to TP (Wang et al., 2020a, 2021), these fixed UVAI hotspots in all the seasons imply the possible existence of local dust activities. In addition, the notable increase in frequency of UVAI >1.0 (>20–30 days) during spring in northeastern and southwestern China are associated with intensive biomass burning smoke. Considering some missing values of UVAI due to cloudy weather, the actual frequency of dust transport can be higher.

Different from the temporary fire smoke, dust-active hotspots over northwestern part of East Asia indicated by UVAI values exhibit basically the same distribution in different seasons (Fig. 4). There are three major dust-active regions including Taklimakan Deserts and its surrounding areas, the Gobi deserts, and deserts in northeastern China, which exhibit distinct features in ground chemical element analysis (Huang et al., 2010). It's well-known that dust storms in East Asia mostly occur in spring due to the strong surface winds and dry weather (Wu et al., 2020). The frequency of UVAI >1.0 during spring exceeds 20–30 days over almost all the bare areas in the northwestern part of East Asia (Fig. 1), and can be higher than 40–50 days in core areas of the dust sources. Although the frequency and spatial scales of dust activities get obviously smaller in other seasons, core sources areas of Taklimakan Desert and Gobi deserts remain very active throughout most time of the year. Considering only several large-scale dust storms found in eastern China every year (Huang et al., 2006, 2010), the unnoticeable but frequent dust plumes as shown in Fig. 2 can be the predominant sources of prevailing dust over downstream regions (Tao et al., 2014).

Dust activities in Taklimakan Desert and Gobi deserts exhibit remarkable differences in both spatial and temporal patterns (Fig. 4). The frequency and spatial scales of dust activities in Taklimakan Desert are much larger than in Gobi deserts. The lowest frequency of UVAI >1.0 in Taklimakan Desert and Gobi deserts appears in winter and summer, respectively, which can be associated with different meteorological and dust uplifting conditions. Dust transport from the deserts to eastern China mainly occurs in winter and spring, exerting the most influence on northern China. There are about 20–40 days of dust transport passing over the northwestern Pacific during winter and spring. In particular, the close frequency of UVAI >1.0 demonstrates considerable transport potential of the dust plumes in winter. It is worth noting that frequency of UVAI >1.0 over downstream northern China, SC, and TP in winter is slightly higher than in spring. One possible reason is that mixing with the accumulated pollution in eastern China can enhance absorption of the passing dust plumes (Kim et al., 2005). Meanwhile, the distinct meteorological conditions such as wind speed and direction in winter and spring as well as their corresponding influence on dust activation and transport process can be another cause.

3.2. Characterization of dust transport with CALIPSO detection and MERRA-2

To explore the transport potential of dust sources in East Asia, CALIPSO aerosol extinction profiles in dust hotspots of Taklimakan Desert and Gobi deserts are compared (Fig. 5). The strongest dust extinction is concentrated within 1–2 km near surface, approximately 2–3 times of that above the planetary boundary layer (PBL). CALIPSO monthly aerosol extinction profiles show that dust particles of the deserts can be uplifted to 4–6 km, and the frequency of their occurrence decreases rapidly with altitudes. Consistent with OMI UVAI, extinction of the elevated dust particles reaches maximum values of 0.3–0.4 km^{-1} in spring. The minimum values of dust extinction appear in winter with also the lowest dust uplifting height. Different from the declining extinction near surface, there is an obvious increase in the amount of elevated dust from March to May. Despite similar heights of the dust layer top, the whole vertical extinction in Gobi deserts is much lower than that in Taklimakan Desert, which is consistent with the low values of satellite AODs. Additionally, dust loading in Gobi deserts can be partly underestimated by the coarse resolution of CALIPSO L3 monthly grid products due to the limited scales of emission hotspot (Fig. 2S).

CALIPSO monthly extinction profiles reveal prevalent aerosol transport above the air pollution in northern China (Fig. 6). During winter and spring, the strong aerosol extinction below 500 m demonstrates the accumulation of local anthropogenic emissions within PBL (Tao et al., 2014). From January, notable peak values of aerosol extinction appear at the heights of 1–3 km over the anthropogenic pollution near surface. As show in the air pollution event in eastern China (Fig. 2c), elevated dust plumes cover over haze layers at altitudes of 1–3 and 3–8 km respectively, and tend to drop and mix with local atmospheric pollutants in transport path. In agreement with the increase in uplifted height of dust in the deserts, dust transport occurs at a much higher altitudes in 1–6 km in northern China during spring. Elevated aerosol layers also exist within 1–4 km in summer and fall, but only appear in a few years during 2007–2018. Besides airborne dust, the seasonal agricultural fire smoke in summer and fall can be one important contributing factor (Tao et al., 2020).

Dust occurrence in CALIPSO vertical detection over northern China is calculated to examine frequency of dust transport (Fig. 7). The occurrence frequency of airborne dust within 3 km and 3–8 km are at very close levels, demonstrating prevailing dust-pollution interaction in northern China. Different from frequency of OMI UVAI >1.0, dust occurrence over northern China in CALIPSO observation is most frequent in spring rather than in winter, especially in the altitudes of 3–8 km. It should be stated that frequency of dust occurrence is considerable during winter within 3 km, which is higher than in fall and summer. Comparison between CALIPSO aerosol and dust occurrence shows that airborne dust accounts for more than 50–80% of the aerosols

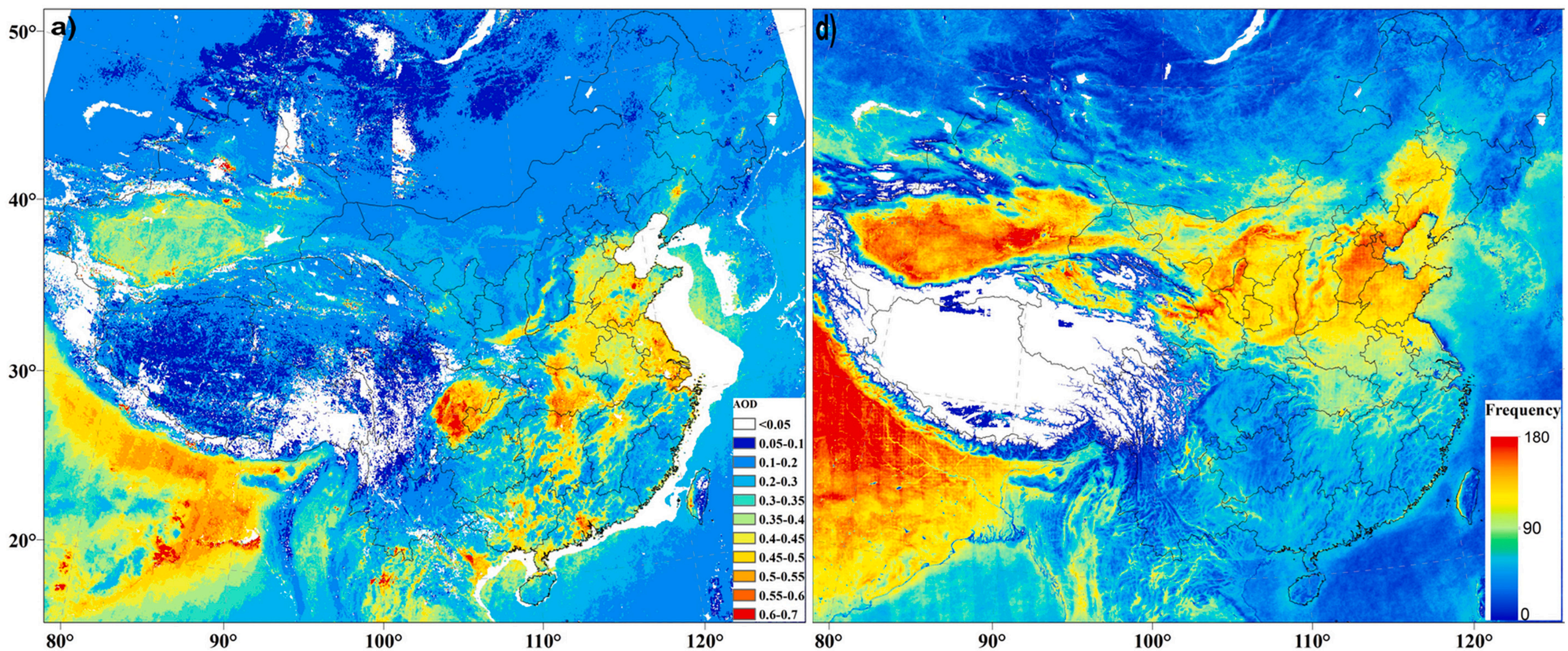

Fig. 3. a) Annual mean of MISR AOD at 550 nm, and b) annual frequency of MODIS MAIAC AOD >0.1 during 2008–2018.

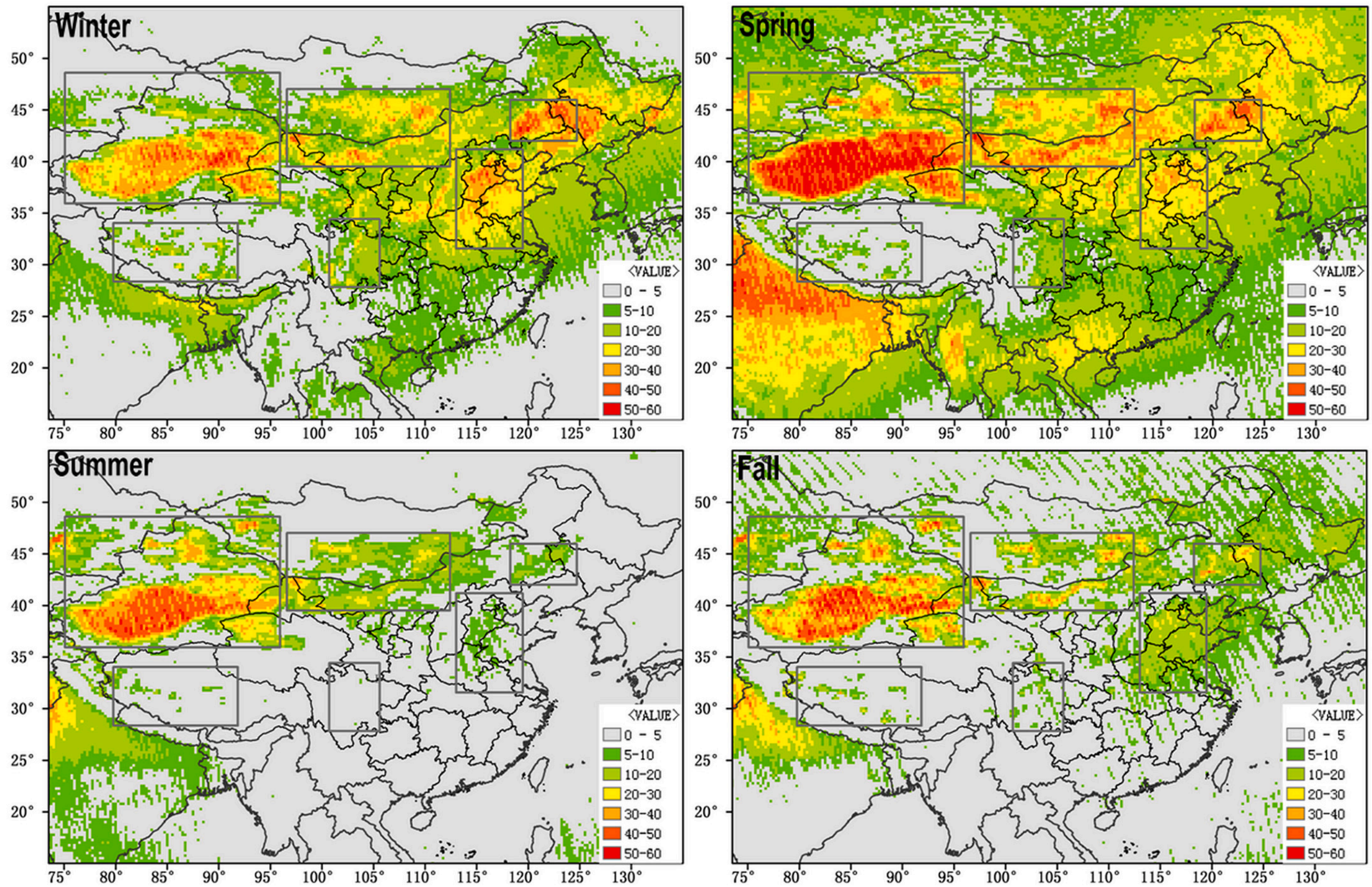

Fig. 4. Seasonal frequency of OMI UVAI >1.0 in winter, spring, summer, and fall of 2005–2008.

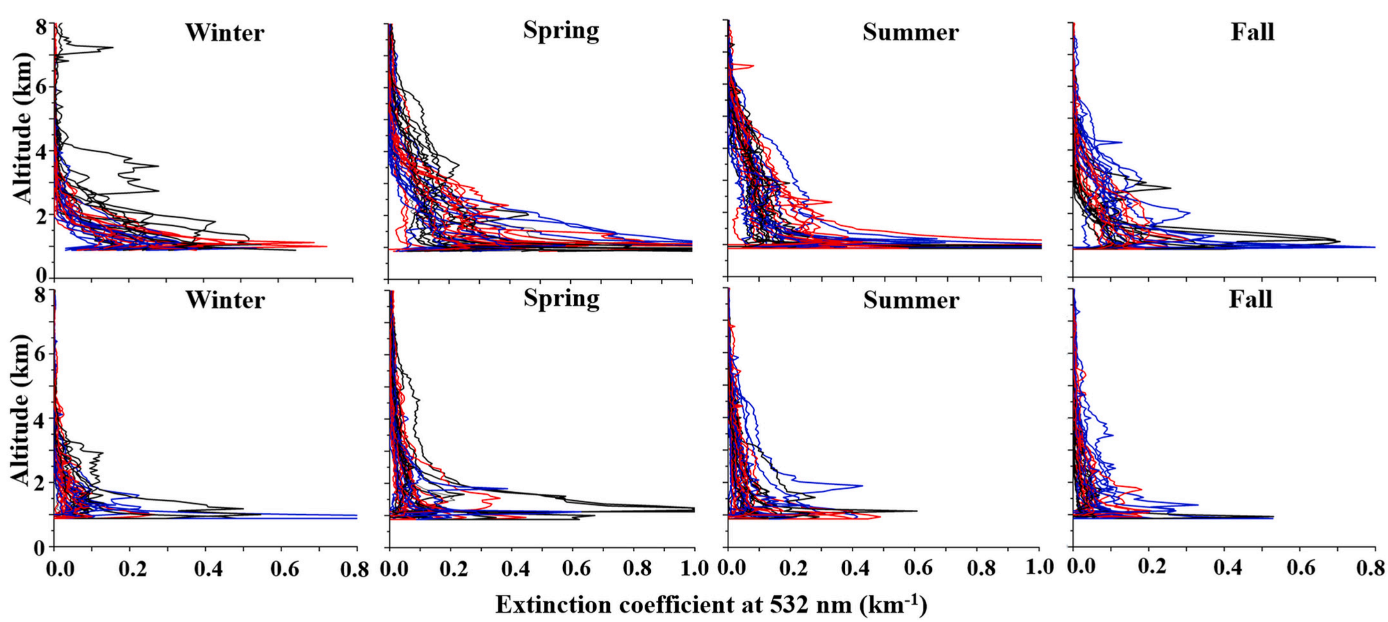

Fig. 5. CALIPSO nighttime monthly mean aerosol extinction profiles at 532 nm in Taklimakan Desert (top, 82.5°E, 38°N) and Gobi deserts (bottom, 107.5°E, 42°N) during 2007–2018. The blue, red, and black lines represent the first, second, third months of the four seasons. (For interpretation of the references to color in this figure legend, the reader is referred to the web version of this article.)

within 3–8 km except in summer. By contrast, fractions of dust particles are mostly lower than one-fourth to one-third in the polluted conditions within 3 km.

Compared with the instantaneous satellite observation, MERRA-2 reanalysis with a space-time continuity has an obvious advantage in characterizing aerosol processes (Guo et al., 2017). Fig. 8 shows

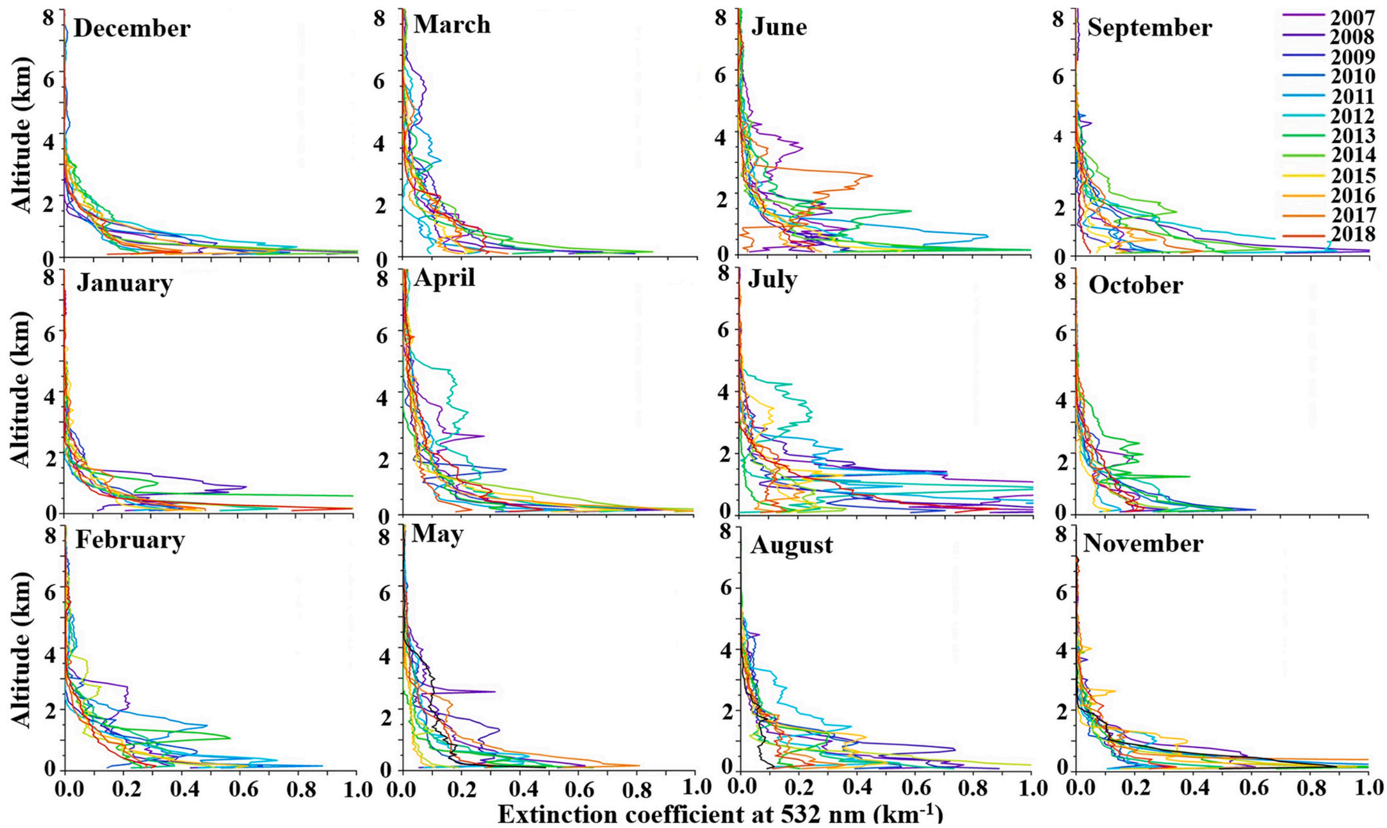

Fig. 6. CALIPSO nighttime monthly mean aerosol extinction profiles at 532 nm in northern China (117.5°E, 38°N) during 2007–2018.

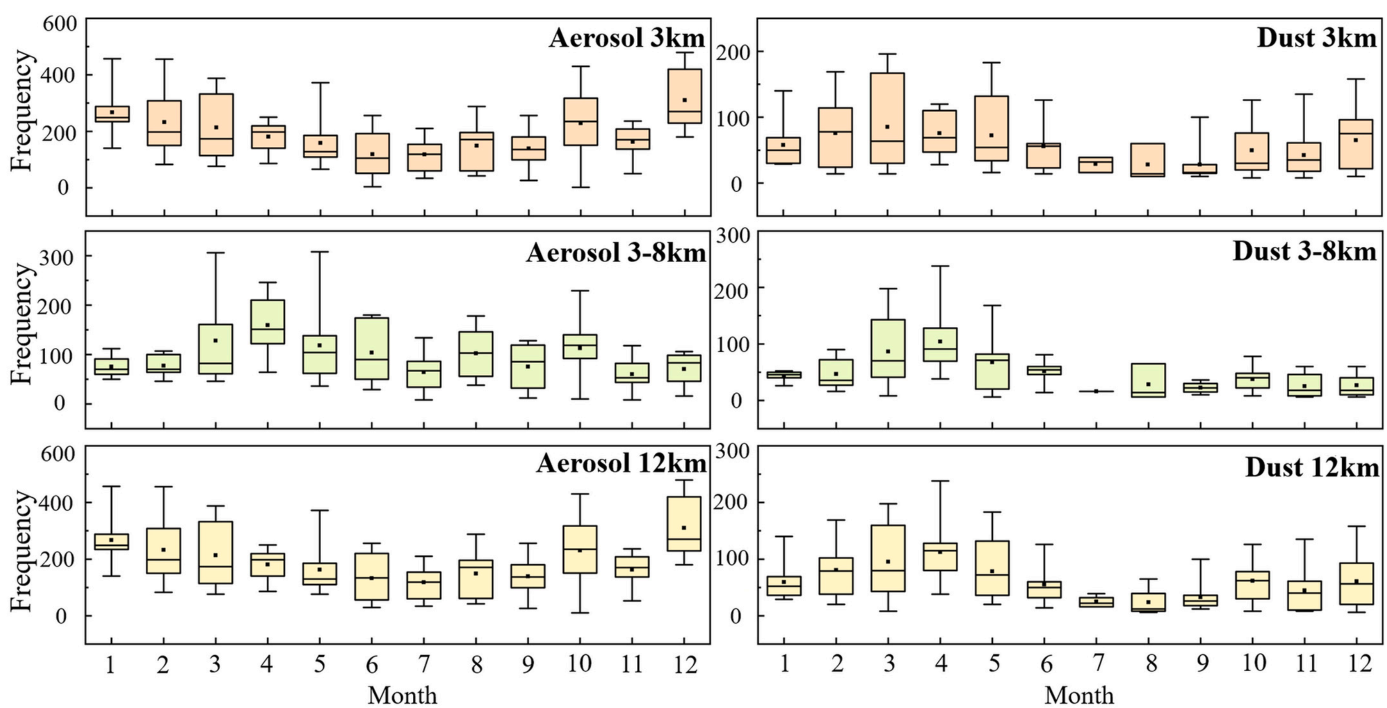

Fig. 7. Aerosol and dust occurrence frequency of in CALIPSO nighttime detection within 3, 3–8, and 12 km in northern China (117.5°E, 38°N) during 2007–2018.

comparison between seasonal MISR AOD and MEERA-2 dust reanalysis. Although MERRA-2 can generally reproduce seasonal variations of dust AOD in the deserts, its spatial patterns exhibit marked difference with MISR AOD's. There is an underestimation by ~0.1 in MERRA-2 dust AOD over the eastern part of the Gobi deserts, where annual MERRA-2 dust emission is very low (< 5 g/m^2) (Fig. 2S). While MERRA-2 obviously underestimates dust AOD over Taklimakan Desert during winter, it exhibits considerable overestimation in the other seasons. Consistent

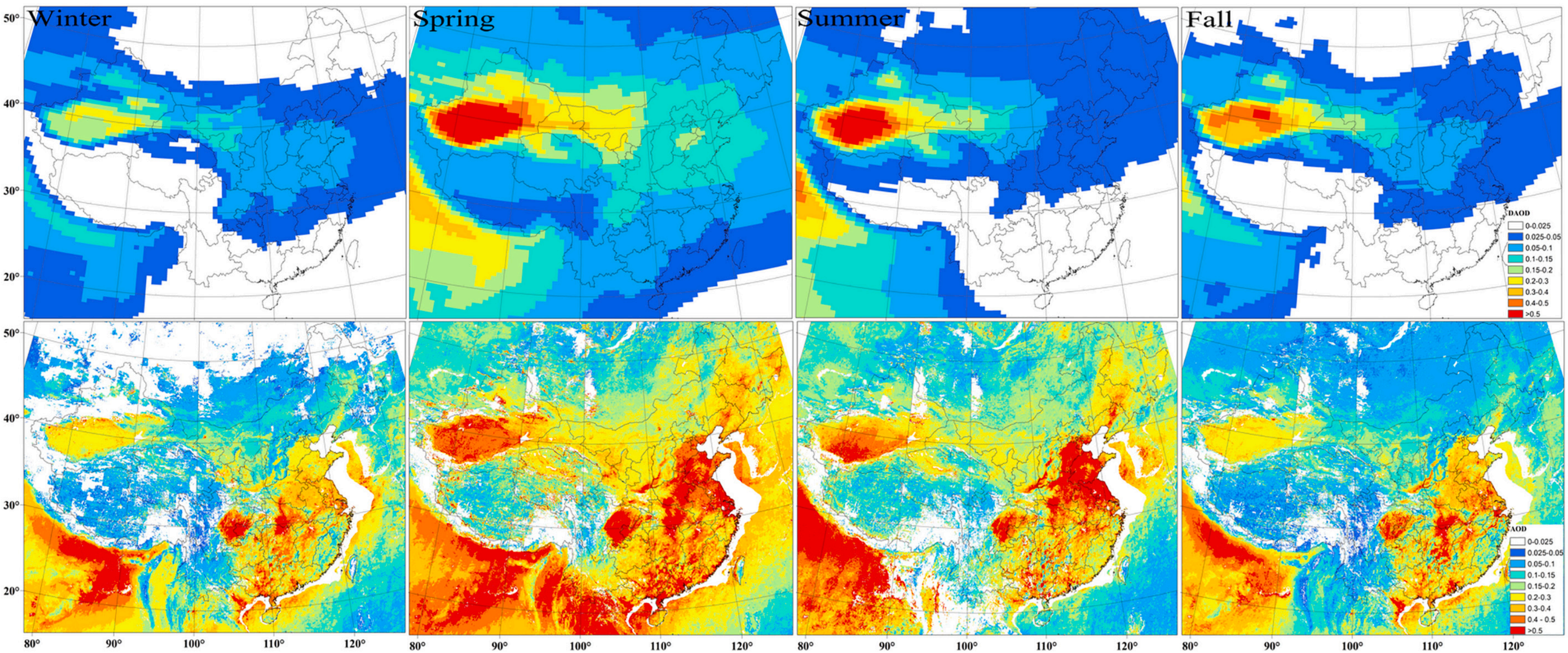

Fig. 8. Annual mean of MERRA-2 dust AOD and MISR AOD at 550 nm in winter, spring, summer, and fall of 2007–2018.

with dust emission, high values of MERRA-2 dust AOD tend to be concentrated in the northern and eastern parts of Taklimakan Desert. By contrast, MISR AOD hotspots are distributed around the edges of Taklimakan Desert, and mainly in the southern part during summer. Seasonal frequency (~50–60 days) of MERRA-2 dust AOD >0.1 over the Sichuan Basin is much higher than that (~10–20 days) of UVAI >1.0 in spring (Fig. 3S), which can largely overestimate transport of dust particles.

MERRA-2 surface dust concentration can reflect both dust activities and their influence on air quality near surface (Fig. 9). Despite the low values of MERRA-2 dust AOD (~0.05–0.1), seasonal mean of MERRA-2 surface dust concentration in the eastern part of East Asia is mostly higher than 10–25 μg/m^3 except in summer. There are totally 60–90 days with surface dust concentration exceeding 30 μg/m^3 in northern China and Sichuan Basin for one year (Fig. 4S). Daily backward trajectories at the altitude of 3 km over northern China reveal that northwestern winds passing over the deserts are predominant except in summer. Most airflows pass over the Gobi deserts, and even these from the Taklimakan Desert. Despite the low frequency of dust activities and limited scales of dust-active areas in Gobi deserts (Fig. 4), the northwesterly air mass and high-altitude terrain (>1 km) give a benefit to downstream transport once strong winds uplifting the mineral dust. By contrast, elevated dust plumes over the active Taklimakan Desert have a high probability of long-range transport when air flows originate from over passing over. There are more than ten days with air masses from Taklimakan Desert at 3 km in northern China except in summer.

3.3. Transport process of typical dust events over East Asia

Although PM_{10} is only one part of the coarse dust particles, its hourly variations compared with fine particles can be an effective indicator for dust events near surface (Fig. 10). PM_{10} in ground sites around Taklimakan Desert and Gobi deserts exhibits very different temporal variations. Besides the striking peak values, PM_{10} in Hotan and Aksu keeps at ~300 μg/m^3 with a flat change, demonstrating consecutive dust emissions in Taklimakan Desert. To explore transport process of the prevalent but unnoticeable dust plumes over East Asia, we select one typical dust event in cloudless days during Dec. 14–17, 2018 by daily OMPS UVAI >1.0 (Fig. 11). While no visible dense dust plumes exist in the satellite true color images, dust sources around Taklimakan Desert are active during the whole period with MODIS AOD >0.3. There is a notable transport path along the southern part of Gobi deserts on Dec. 14, 2018. With prevailing northwestern winds at 700 hPa (~3 km) over the dust sources, OMPS UVAI shows obvious dust plumes over the haze pollution in eastern China. When southwest airflows appear over eastern China on Dec. 14–15, the northwesterly dust plumes are trapped over northern China. Then, these dust plumes pass through eastern China, and move southeastward on Dec. 16–17 when northwestern winds are predominant (Fig. 11).

Fig. 12 shows variations of PM_{10} and collocated MERRA-2 surface dust concentration in ground sites near Gobi deserts and downstream regions. Variations of MERRA-2 surface dust concentration include 5–6 fast peak processes in Bayan Nur (>500 μg/m^3) and Ordos (>300 μg/m^3) near the Gobi deserts during Dec. 15–23. However, PM_{10} in these two sites is much lower with only a slight increase, demonstrating that MERRA-2 largely overestimates the surface dust concentration in Gobi deserts. When dust plumes pass over Zaozhuang in eastern China on Dec. 16, there is a marked increase in the difference between PM_{10} and $PM_{2.5}$ ($PM_{10\text{-}2.5}$). Although dust transport also covers Huaian and Pingdingshan, changes of $PM_{10\text{-}2.5}$ during Dec. 14–17 is not obvious, with a little deposition. As shown in Fig. 2, these elevated dust plumes can be separated from anthropogenic pollution near surface. The most prominent dust event during December 2018 occurs in the first week, with a large increase in $PM_{10\text{-}2.5}$ at all the sites in Figs. 10 and 12. Dust storm with PM_{10} exceeding 800 μg/m^3 first appears in Taklimakan Desert on Dec.1, and then moves to the Gobi deserts the next day. When dust plumes are blown downstream to eastern China and the Sichuan Basin on Dec. 3–5, the peak of $PM_{10\text{-}2.5}$ appears in Pingdingshan (~500 μg/m^3), Mianyang (~200 μg/m^3), and Zaozhuang (~150 μg/m^3).

Daily variations of dust transport in satellite and ground observations provide a direct view of MERRA-2's performance in characterizing these frequent dust plumes. Fig. 13 displays variations of MERRA-2 dust AOD, surface concentration, and column mass concentration at 14:00 local time during Dec. 14–17, 2018. Spatial patterns of MERRA-2 dust AOD and MODIS results exhibit remarkable difference (Fig. 11). MODIS AOD reveals marked dust hotspots in the western and eastern Taklimakan Desert, but high values of MERRA-2 dust AOD are concentrated in the northern part. Consistent with the low values of dust emissions (Fig. S2), MERRA-2 obviously underestimates surface dust concentration in southern Taklimakan Desert. Meanwhile, PM_{10} near Gobi deserts is at ~50 μg/m^3 with large daily fluctuations, which has been largely overestimated in MERRA-2. Considerable uncertainties exist in both the magnitude and process of MERRA-2 dust reanalysis in East Asia.

3.4. Discussion

Consistent with variations of ground PM_{10} around the deserts, satellite observations including UVAI and AOD clearly reveal spatial patterns of dust-active areas as well as frequency and scales of their dust activities (Figs. 3 and 4). The dust transport potential of Taklimakan Desert and Gobi deserts has been compared in several previous studies. While analysis based on model simulation considers a larger influence of Gobi deserts over East Asia (Chen et al., 2017), observational study with MISR dust plume top height and motion vectors suggests a higher transport potential in Taklimakan Desert with lower wind speed required for dust uplifting and smaller particle sizes (Yu et al., 2019). Comparison with satellite observations shows that MERRA-2 reanalysis obviously overestimates the dust loading in Gobi deserts and underestimate in the western and southern Taklimakan Desert. Unlike the always active dust sources in Taklimakan Desert, variations of ground PM_{10} show few dust events near Gobi deserts in winter, indicating stronger surface winds required to activate the dust emission in Gobi deserts. Furthermore, the very low values (< 0.1 km^{-1}) of CALIPSO mean extinction profiles above 3 km over Gobi deserts imply few intense dust events with long-range transport potential (Fig. 5), even in spring.

CALIPSO observations have shown prevalent dust plumes overlaying over the haze layers in eastern China with dynamic mixing states during winter and spring (Fig. 6). Although fine particles are predominant in air pollution near surface, coarse particles account for a larger fraction in columnar volume size distribution (Tao et al., 2014). Ground chemical analysis of dust events shows that dust particles can mix with atmospheric pollutants on the pathway of transport (Huang et al., 2010). Dust storms with strong surface winds can clean up local anthropogenic pollution within a short time and bring out deposition of a large amount of coarse dust particles. By contrast, transport of frequent dust plumes at smaller scales usually occurs above the accumulated haze layers near surface in winter and spring because the predominant northwestern winds at 700 hPa cannot reach the PBL bottom. During winter and early spring, the low surface temperature tends to trap local pollution below 500 m near surface by intense temperature inversion (Fig. 5S), which can weaken and delay the mixing of dust-pollution (Tao et al., 2021).

The current MERRA-2 reanalysis has some uncertainties in characterizing dust loading and transport process of the prevalent dust plumes over East Asia. It should be noted that MODIS DB AOD used in MERRA-2 data assimilation exhibits large underestimation in low and moderate values (< 0.5) in the deserts of East Asia (Tao et al., 2019). As shown in Fig. 11, assimilation of satellite AOD with higher accuracy could favor the improvement of dust simulations (Wang et al., 2012). The distinct dust and surface properties in Taklimakan Desert and Gobi deserts needs more observational studies. Recent geostationary satellite with a high temporal resolution and polar satellite with multi-angle polarized measurements can provide more information on characterizing dust

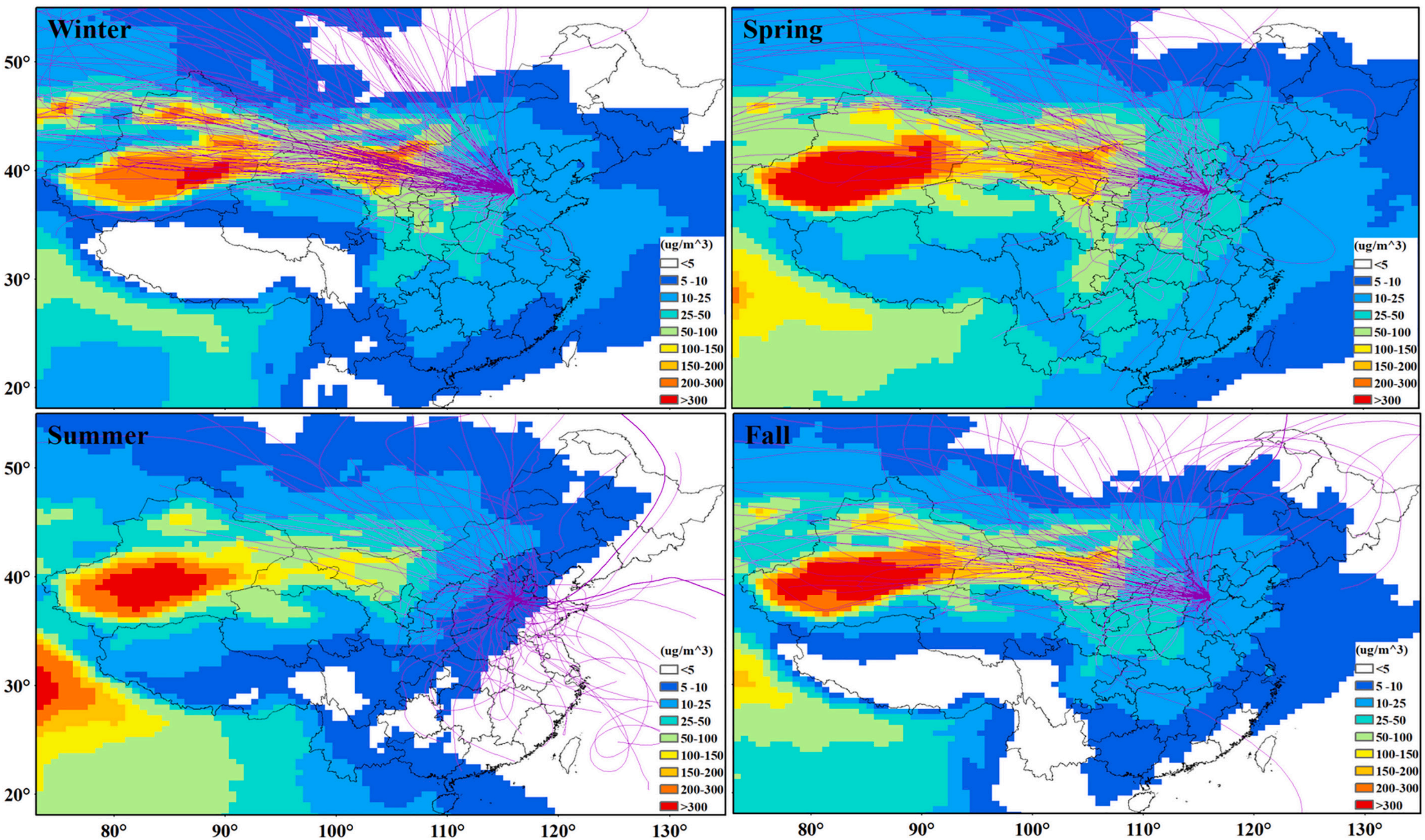

Fig. 9. Seasonal MEERA-2 dust surface concentration in winter, spring, summer, and fall of 2007–2018. The purple lines denote daily backward trajectories in 72 h at the altitude of 3 km in northern China (116°E, 38°N). (For interpretation of the references to color in this figure legend, the reader is referred to the web version of this article.)

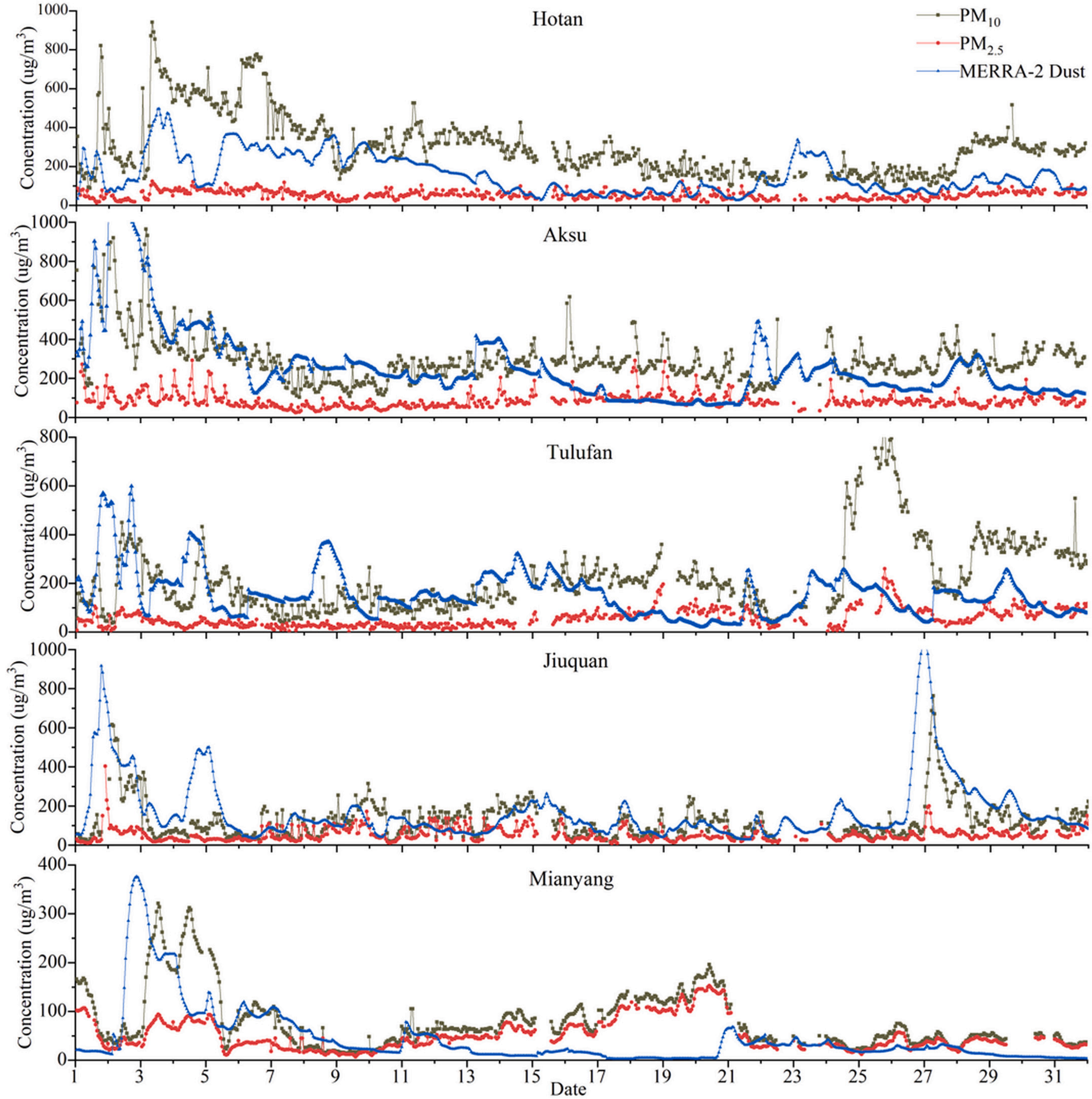

Fig. 10. Hourly concentration of PM_{10} (black), $PM_{2.5}$ (red), and MERRA-2 surface dust concentration (blue) in Hotan, Aksu, Tulufan, Jiuquan, and Mianyang during December 2018. (For interpretation of the references to color in this figure legend, the reader is referred to the web version of this article.)

activities over East Asia.

4. Conclusions

The intense dust storms from the deserts of East Asia have caused widely attention due to their trans-pacific transport. However, there are only a few dust storms usually concentrated in spring every year, which cannot explain the prevalent dust particles over East Asia. To understand the predominant dust events determining spatial patterns of the airborne dust, we present an observational insight into dust activities and their downstream transport over East Asia with combined satellite observations and MERRA-2 reanalysis. Based on the frequency of MODIS AOD >0.1 and OMI UVAI >1.0, it's found that unnoticeable but frequent dust plumes are the dominant sources of the prevailing dust aerosols over East Asia. These dust plumes are usually transported to eastern China and Sichuan Basin during winter and spring within 3–5 days once favorable meteorological conditions appear. Unlike the year-round active dust hotspots over the vast Taklimakan Desert, dust activities in the scattered Gobi deserts are at much smaller scales and lower frequency due to stronger winds needed for dust uplifting.

The heights of elevated dust plumes over the deserts are concentrated within 2–6 km with large monthly variations. Compared with the

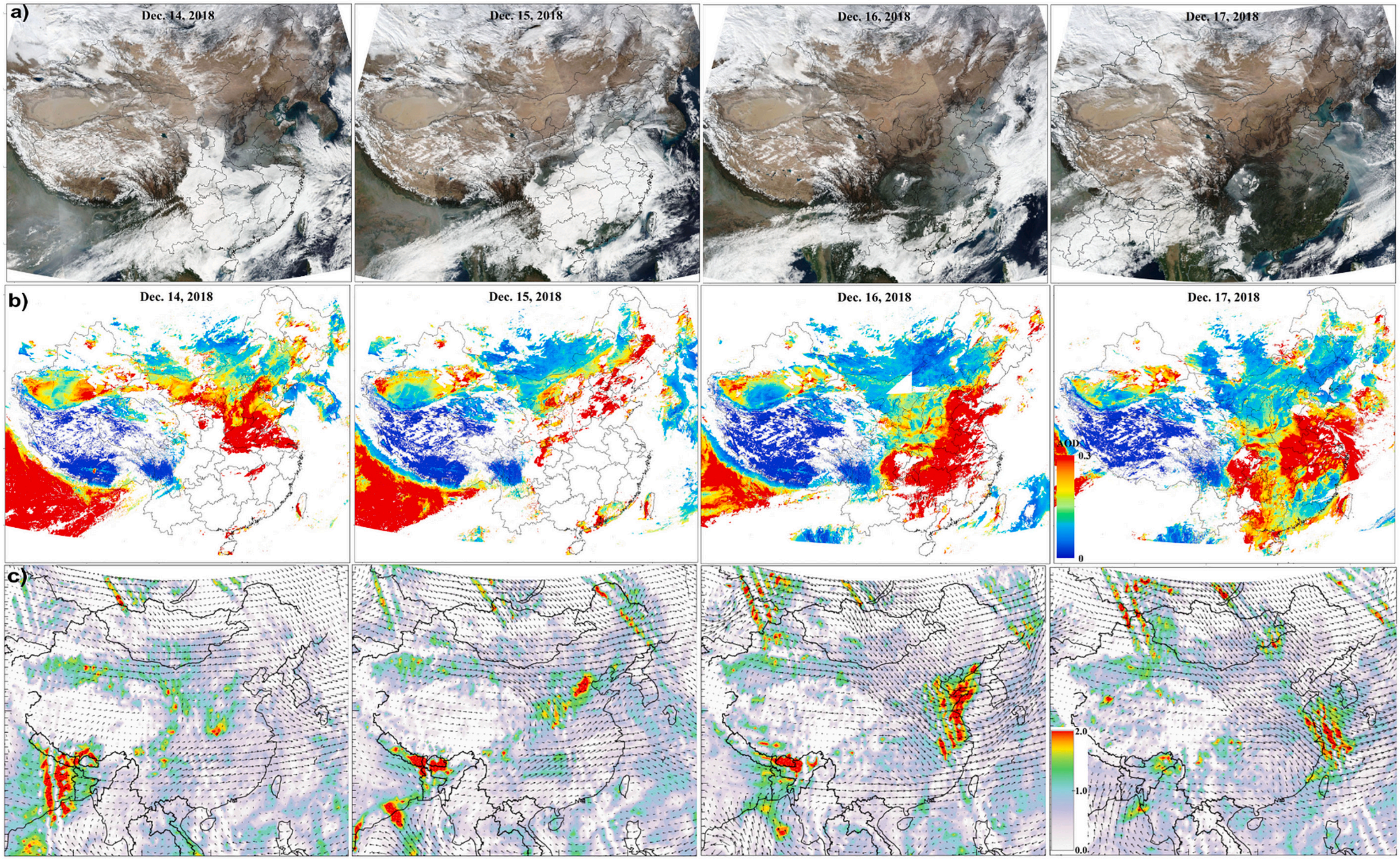

Fig. 11. a) VIIRS true color image, b) MODIS MAIAC AOD at 550 nm, c) OMPS UVAI with winds at 700 hPa during Dec. 14–17, 2018.

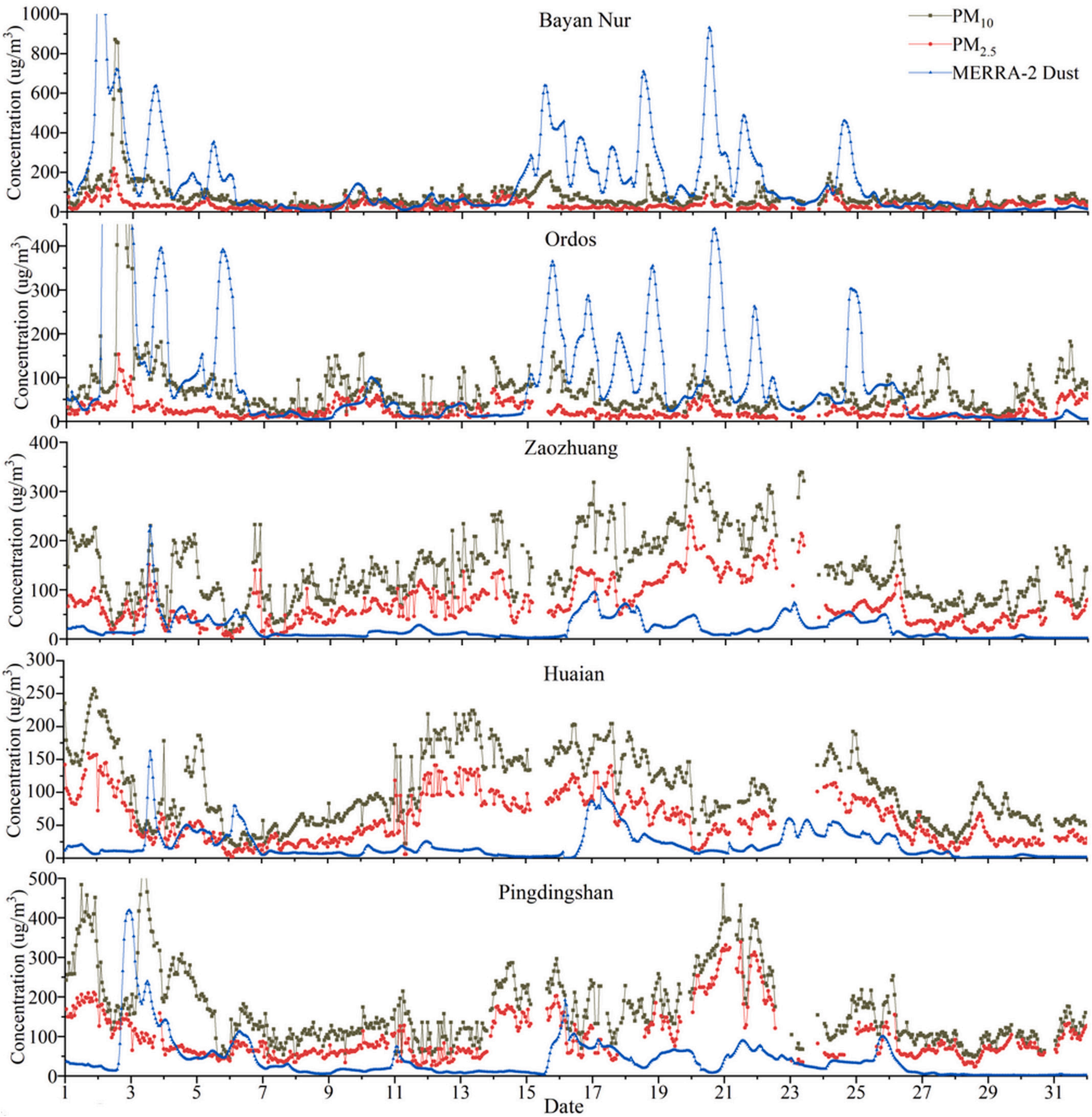

Fig. 12. Same as Fig. 10 but for ground sites in Bayan Nur, Ordos, Zaozhuang, Huaian, and Pingdingshan.

notable peak values of dust plumes over Taklimakan Desert, the very low mean values (< 0.1 km^{-1}) of dust extinction above 3 km over Gobi deserts demonstrate few intense dust events with long-range transport potential. Unlike dust storms with strong winds cleaning up the surface air pollution, these dust plumes usually overlay over the haze layers in eastern China. The common temperature inversions in eastern China during winter and early spring can favor a delaying mixing of dust-pollution.

The current MERRA-2 reanalysis tends to overestimate dust loading in the Gobi deserts and underestimate in the Taklimakan Desert. Also, spatial locations of MERRA-2 dust emission hotspots exhibit obvious discrepancy with some results of the satellite observations. Satellite and ground observations with higher accuracy and more information are in need to improve dust uplifting mechanism in different deserts, knowledge of their chemical and physical properties, and to constrain the model simulations.

Data availability statement

The original MODIS, OMI, OMPS, CALIPSO and MERRA-2 data (https://disc.gsfc.nasa.gov) and MISR aerosol products (https://misr.jpl.nasa.gov) can be downloaded from the website by registering a user account for free. The air quality data and results presented in this manuscript will be made available through Coalition on Publishing Data

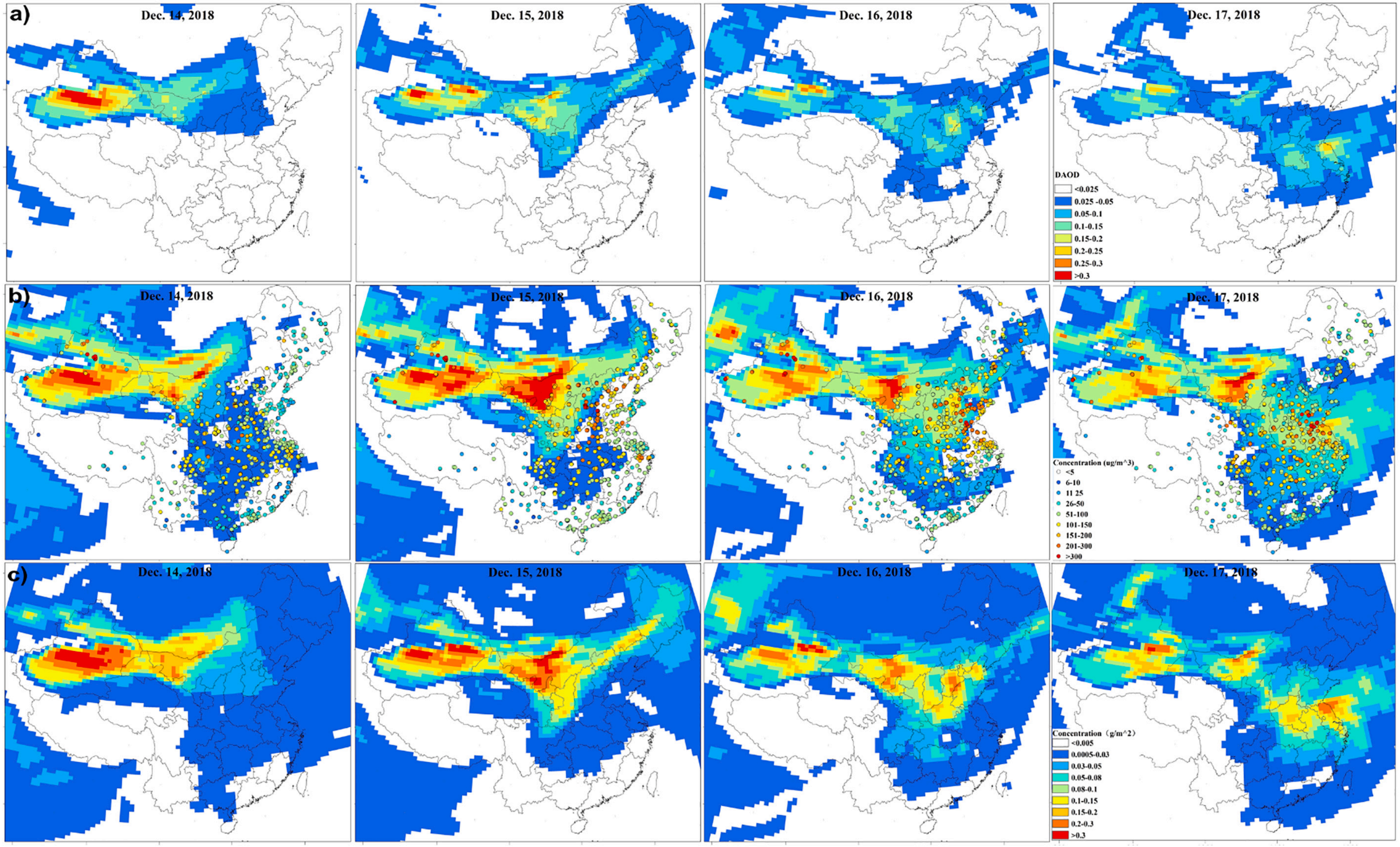

Fig. 13. MERRA-2 a) dust AOD, b) surface dust concentration, c) columnar dust concentration during Dec. 14–17, 2018.

in the Earth and Space Sciences (https://copdessdirectory.osf.io) and please email M. Tao (taomh@cug.edu.cn) for details.

Declaration of Competing Interest

The authors declare that they have no known competing financial interests or personal relationships that could have appeared to influence the work reported in this paper.

Acknowledgments

This study was supported by National Natural Science Foundation of China (Grant No. 41871262 and 41830109). Jun Wang's participation is made possible via the in-kind support from the University of Iowa. We thank the MODIS, MISR, OMI, and OMPS team for the data used.

Appendix A. Supplementary data

Supplementary data to this article can be found online at https://doi.org/10.1016/j.atmosres.2021.105886.

References

Buchard, V., Randles, C., Da Silva, A., Darmenov, A., Colarco, P., Govindaraju, R., Ferrare, R., Hair, J., Beyersdorf, A., Ziemba, L., 2017. The MERRA-2 aerosol reanalysis, 1980 onward. Part II: evaluation and case studies. J. Clim. 30 (17), 6851–6872.

Chen, S., Huang, J., Li, J., Jia, R., Jiang, N., Kang, L., Ma, X., Xie, T., 2017. Comparison of dust emissions, transport, and deposition between the Taklimakan Desert and Gobi Desert from 2007 to 2011. Sci. China Earth Sci. 60 (7), 1338–1355.

Dentener, F.J., Carmichael, G.R., Zhang, Y., Lelieveld, J., Crutzen, P.J., 1996. Role of mineral aerosol as a reactive surface in the global troposphere. J. Geophys. Res. Atmos. 101 (D17), 22,869–22,889. https://doi.org/10.1029/96JD01818.

Gelaro, R., McCarty, W., Suárez, M.J., Todling, R., Molod, A., Takacs, L., et al., 2017. The modern-era retrospective analysis for research and applications, version 2 (MERRA-2). J. Clim. 30 (14), 5419–5454.

Ginoux, P., Prospero, J.M., Gill, T.E., Hsu, N.C., Zhao, M., 2012. Global-scale attribution of anthropogenic and natural dust sources and their emission rates based on MODIS Deep Blue aerosol products. Rev. Geophys. 50 (3), RG3005.

Guo, J., Lou, M., Miao, Y., Wang, Y., Zeng, Z., Liu, H., He, J., Xu, H., Wang, F., Min, M., Zhai, P., 2017. Trans-Pacific transport of dust aerosols from East Asia: Insights gained from multiple observations and modeling. Environ. Pollut. 230, 1030–1039.

Herman, J.R., Bhartia, P.K., Torres, O., Hsu, C., Seftor, C., Celarier, E., 1997. Global distribution of UV-absorbing aerosols from Nimbus 7/TOMS data. J. Geophys. Res. Atmos. 102 (D14), 16911–16922.

Huang, J., Lin, B., Minnis, P., Wang, T., Wang, X., Hu, Y., Yi, Y., Ayers, J.K., 2006. Satellite-based assessment of possible dust aerosols semi-direct effect on cloud water path over East Asia. Geophys. Res. Lett. 33 (19), L19802.

Huang, K., Zhuang, G., Li, J., Wang, Q., Sun, Y., Lin, Y., Fu, J.S., 2010. Mixing of Asian dust with pollution aerosol and the transformation of aerosol components during the dust storm over China in spring 2007. J. Geophys. Res. Atmos. 115 https://doi.org/10.1029/2009JD013145. D00K13.

Huang, J., Wang, T., Wang, W., Li, Z., Yan, H., 2014. Climate effects of dust aerosols over East Asian arid and semiarid regions. J. Geophys. Res. Atmos. 119 (19), 11,398–311,416.

Itahashi, S., Yumimoto, K., Uno, I., Eguchi, K., Takemura, T., Hara, Y., Shimizu, A., Sugimoto, N., Liu, Z., 2010. Structure of dust and air pollutant outflow over East Asia in the spring. Geophys. Res. Lett. 37, L20806 https://doi.org/10.1029/2010GL044776.

Jickells, T.D., et al., 2005. Global iron connections between desert dust, ocean biogeochemistry, and climate. Science 308 (5718), 67–71.

Jin, S., Ma, Y., Gong, W., Liu, B., Fan, R., 2021a. Characteristics of vertical atmosphere based on five-year microwave remote sensing data over Wuhan region. Atmos. Res. 105710.

Jin, S., Zhang, M., Ma, Y., Gong, W., Shi, Y., 2021b. Adapting the dark target algorithm to advanced MERSI sensor on the FengYun-3-D satellite: retrieval and validation of aerosol optical depth over land. IEEE Trans. Geosci. Remote Sens. 99, 1–17.

Kahn, R.A., Gaitley, B.J., 2015. An analysis of global aerosol type as retrieved by MISR. J. Geophys. Res. Atmos. 120 (9), 4248–4281.

Kim, D.-H., Sohn, B.J., Nakajima, T., Takamura, T., 2005. Aerosol radiative forcing over east Asia determined from ground-based solar radiation measurements. J. Geophys. Res. Atmos. 110 https://doi.org/10.1029/2004JD004678. D10S22.

Kim, D., Chin, M., Yu, H., Pan, X., Bian, H., Tan, Q., Kahn, R.A., Tsigaridis, K., Bauer, S. E., Takemura, T., Pozzoli, L., 2019. Asian and Trans-Pacific Dust: a Multimodel and Multiremote Sensing Observation Analysis. J. Geophys. Res. Atmos. 124 (23), 13534–13559.

Lyapustin, A., Wang, Y., Korkin, S., Huang, D., 2018. MODIS Collection 6 MAIAC algorithm. Atmos. Meas. Tech. 11 (10), 5741–5765.

Ma, J., Chen, Y., Wang, W., Yan, P., Liu, H., Yang, S., Hu, Z., Lelieveld, J., 2010. Strong air pollution causes widespread haze-clouds over China. J. Geophys. Res. Atmos. 115, D18204 https://doi.org/10.1029/2009JD013065.

Ma, Y., Zhang, M., Jin, S., Gong, W., Chen, N., Chen, Z., Jin, Y., Shi, Y., 2019. Long-term investigation of aerosol optical and radiative characteristics in a typical megacity of Central China during winter haze periods. J. Geophys. Res. Atmos. 124.

Omar, A.H., D, M., Winker, C., Kittaka, M.A., Vaughan, Z., Liu, Y., Hu, Y., C, R., Trepte, R.R., Rogers, R.A., Ferrare, K., Lee, R.E., Kuehn, Hostetler, C.A., 2009. The CALIPSO automated aerosol classification and lidar ratio selection algorithm. J. Atmos. Ocean. Technol. 26 (10), 1994–2014.

Tackett, J.L., Winker, D.M., Getzewich, B.J., Vaughan, M.A., Young, S.A., Kar, J., 2018. CALIPSO lidar level 3 aerosol profile product: version 3 algorithm design. Atmos. Meas. Tech. 11 (7), 4129–4152.

Tao, M., Chen, L., Su, L., Tao, J., 2012. Satellite observation of regional haze pollution over the North China Plain. J. Geophys. Res. Atmos. 117 (D12), D12203.

Tao, M., Chen, L., Wang, Z., Ma, P., Tao, J., Jia, S., 2014. A study of urban pollution and haze clouds over northern China during the dusty season based on satellite and surface observations. Atmos. Environ. 82 (0), 183–192.

Tao, M., Wang, J., Li, R., Wang, L., Wang, L., Wang, Z., Tao, J., Che, H., Chen, L., 2019. Performance of MODIS high-resolution MAIAC aerosol algorithm in China: Characterization and limitation. Atmos. Environ. 213, 159–169.

Tao, M., Wang, J., Li, R., Chen, L., Xu, X., Wang, L., et al., 2020. Characterization of aerosol type over East Asia by 4.4 km MISR product: first insight and general performance. J. Geophys. Res. Atmos. 125 https://doi.org/10.1029/2019JD031909 e2019JD031909.

Tao, M., Gui, L., Li, R., Wang, L., Liang, S., Li, Q., Wang, L., Yu, C., Chen, L., 2021. Tracking prevailing dust aerosol over the air pollution in Central China with integrated satellite and ground observations. Atmos. Environ. 253, 118369.

Torres, O., Tanskanen, A., Veihelmann, B., Ahn, C., Braak, R., Bhartia, P.K., Veefkind, P., Levelt, P., 2007. Aerosols and surface UV products from Ozone Monitoring Instrument observations: an overview. J. Geophys. Res. Atmos. 112 (D24). D24S47.

Wang, W., Huang, J., Minnis, P., Hu, Y., Li, J., Huang, Z., Ayers, J.K., Wang, T., 2010. Dusty cloud properties and radiative forcing over dust source and downwind regions derived from A-Train data during the Pacific Dust Experiment. J. Geophys. Res. Atmos. 115 https://doi.org/10.1029/2010JD014109. D00H35.

Wang, J., Xu, X., Henze, K., Zeng, J., Ji, Q., Tsay, S.-C., Huang, J., 2012. Top-down estimate of dust emissions through integration of MODIS and MISR aerosol retrievals with the GEOS-Chem adjoint model. Geophys. Res. Lett. 39, L08802 https://doi.org/10.1029/2012GL051136.

Wang, T., Chen, Y., Gan, Z., Han, Y., Li, J., Huang, J., 2020a. Assessment of dominating aerosol properties and their long-term trend in the Pan-Third Pole region: a study with 10-year multi-sensor measurements. Atmos. Environ. 239, 117738.

Wang, T., Han, Y., Huang, J., Sun, M., Jian, B., Huang, Z., Yan, H., 2020b. Climatology of dust-forced radiative heating over the Tibetan Plateau and its surroundings. J. Geophys. Res. Atmos. 125 https://doi.org/10.1029/2020JD032942 e2020JD032942.

Wang, T., Tang, J., Sun, M., Liu, X., Huang, Y., Huang, J., Han, Y., Cheng, Y., Huang, Z., Li, J., 2021. Identifying a transport mechanism of dust aerosols over South Asia to the Tibetan Plateau: a case study. Sci. Total Environ. 758, 143714.

Wu, M.X., Liu, H., Yu, H., Wang, Y., Shi, K., Yang, A., Darmenov, C., Wu, Z., Wang, T., Luo, Y., Feng, Ke, Z., 2020. Understanding processes that control dust spatial distributions with global climate models and satellite observations. Atmos. Chem. Phys. 20 (22), 13835–13855.

Yu, H., Remer, L.A., Chin, M., Bian, H., Tan, Q., Yuan, T., Zhang, Y., 2012. Aerosols from overseas rival domestic emissions over North America. Science 337 (6094), 566–569.

Yu, Y., Kalashnikova, O.V., Garay, M.J., Notaro, M., 2019. Climatology of Asian dust activation and transport potential based on MISR satellite observations and trajectory analysis. Atmos. Chem. Phys. 19 (1), 363–378.

Zhang, X.Y., Arimoto, R., An, Z.S., 1997. Dust emission from Chinese desert sources linked to variations in atmospheric circulation. J. Geophys. Res. Atmos. 102 (D23), 28041–28047.